



MISSOURI  
**S&T**

# CENTER FOR TRANSPORTATION INFRASTRUCTURE AND SAFETY

## **Validation of Coaxial Cable Sensors for Dynamic Crack Detection in RC Columns Under Blast Loads**

by

G. Chen, Ph.D., P.E.

B. Wood, EIT.

J. Baird, Ph.D.

Igor Izyumin

D. Pommerenke, Ph.D.

Note: This document reports findings from a research project titled  
“Concrete Crack and Spalling Detection in a 6.1-meter Precast RC Piles  
with Novel Distributed Cable Sensors and ETDR Measurement”



**NUTC  
R207**

**A National University Transportation Center  
at Missouri University of Science & Technology**

## ***Disclaimer***

The contents of this report reflect the views of the author(s), who are responsible for the facts and the accuracy of information presented herein. This document is disseminated under the sponsorship of the Department of Transportation, University Transportation Centers Program and the Center for Transportation Infrastructure and Safety NUTC program at the Missouri University of Science & Technology, in the interest of information exchange. The U.S. Government and Center for Transportation Infrastructure and Safety assumes no liability for the contents or use thereof.

### Technical Report Documentation Page

1. Report No.  NUTC R207	2. Government Accession No.	3. Recipient's Catalog No.	
4. Title and Subtitle  Validation of Coaxial Cable Sensors for Dynamic Crack Detection in RC Columns Under Blast Loads		5. Report Date  July 2008	
		6. Performing Organization Code	
7. Author/s  G. Chen, Ph.D., P.E., B. Wood, EIT., J. Baird, Ph.D., Igor Izyumin, D. Pommerenke, Ph.D.		8. Performing Organization Report No.  00017865	
9. Performing Organization Name and Address  Center for Transportation Infrastructure and Safety/NUTC program Missouri University of Science & Technology 220 Engineering Research Lab Rolla, MO 65409		10. Work Unit No. (TRAIS)	
		11. Contract or Grant No.  DTRT06-G-0014	
12. Sponsoring Organization Name and Address  U.S. Department of Transportation Research and Special Programs Administration 400 7 <sup>th</sup> Street, SW Washington, DC 20590-0001		13. Type of Report and Period Covered  Final	
		14. Sponsoring Agency Code	
15. Supplementary Notes			
16. Abstract  This study is aimed at validating the sensitivity and resolution of topology-based cable sensors with field testing of three columns, conducting the proof-of-concept tests of an Electrical Time-Domain Reflectometry (ETDR) measurement instrument for real-time detection of the location and time of cracks under cyclic loading, and detecting cracks in RC columns and correlating crack measurements with the strain values on nearby reinforcing bars. To achieve the project objectives, three columns were tested under blast loads: one control specimen and two retrofitted specimens. One cable sensor was installed on the rear (tension) face of each column prior to any strengthening. Proof-of concept blast tests indicated that the sensor and ETDR measurement instrument used during the tests shows the overall distribution of cracks and the location of plastic hinges. The sensitivity of the sensors for crack detection is high in comparison with the noise level. However, the local peaks were not observed for individual cracks due to the limited spatial resolution associated with the measurement instrument used during the blast tests. In the plastic hinge area, the time history of crack opening and closing corresponds well with the strain change measured from the nearby steel reinforcing bar. The large cracks observed during the blast were also seen after the blast was over, indicating the "memory" feature as observed from slowly loaded columns.			
17. Key Words  Concrete, spalling, cable sensors, precast rc piles	18. Distribution Statement  No restrictions. This document is available to the public through the National Technical Information Service, Springfield, Virginia 22161.		
19. Security Classification (of this report)  unclassified	20. Security Classification (of this page)  unclassified	21. No. Of Pages  37	22. Price

**Final Report**  
Agreement No. 59A0571

**VALIDATION OF COAXIAL CABLE SENSORS FOR DYNAMIC CRACK  
DETECTION IN RC COLUMNS UNDER BLAST LOADS**

CALIFORNIA DEPARTMENT OF TRANSPORTATION  
Division of Engineering Services, MS 9-2/51  
P.O. Box 168041  
Sacramento, CA 95816

BY: G. Chen, Ph.D., P.E.  
B. Wood, EIT.  
J. Baird, Ph.D.  
Igor Izyumin  
D. Pommerenke, Ph.D.

Acknowledgments:  
Center for Transportation Infrastructure and Safety  
Missouri University of Science and Technology

DATE SUBMITTED: July 4, 2008

The opinions, findings, and conclusions expressed in this publication are those of the principal investigators and the California Department of Transportation. They are not necessarily those of the U.S. Department of Transportation, Federal Highway Administration. This report does not constitute a standard or regulation.

## **ABSTRACT**

This study is aimed at validating the sensitivity and resolution of topology-based cable sensors with field testing of three columns, conducting the proof-of-concept tests of an Electrical Time-Domain Reflectometry (ETDR) measurement instrument for real-time detection of the location and time of cracks under cyclic loading, and detecting cracks in RC columns and correlating crack measurements with the strain values on nearby reinforcing bars. To achieve the project objectives, three columns were tested under blast loads: one control specimen and two retrofitted specimens. One cable sensor was installed on the rear (tension) face of each column prior to any strengthening. Proof-of-concept blast tests indicated that the sensor and ETDR measurement instrument used during the tests shows the overall distribution of cracks and the location of plastic hinges. The sensitivity of the sensors for crack detection is high in comparison with the noise level. However, the local peaks were not observed for individual cracks due to the limited spatial resolution associated with the measurement instrument used during the blast tests. In the plastic hinge area, the time history of crack opening and closing corresponds well with the strain change measured from the nearby steel reinforcing bar. The large cracks observed during the blast were also seen after the blast was over, indicating the “memory” feature as observed from slowly loaded columns.

## **ACKNOWLEDGEMENT**

Financial support to complete this part of the overall study was provided by California Department of Transportation and Center for Transportation Infrastructure and Safety at Missouri University of Science and Technology. Thanks are due to Jason Cox, Travis Hernandez, and Jeff Bradshaw for their assistance in specimen and test preparations.

## TABLE OF CONTENTS

	Page
ABSTRACT.....	ii
ACKNOWLEDGEMENT .....	iii
LIST OF ILLUSTRATIONS.....	v
1. INTRODUCTION .....	1
2. BACKGROUND OF COAXIAL CABLE CRACK SENSORS.....	1
2.1. Design and Measurement.....	1
2.2. Use for Dynamic Measurement .....	3
3. SPECIMEN DESIGN .....	4
3.1. Three-Column Specimen .....	4
3.2. Capacity Analysis .....	5
4. CONSTRUCTION AND EXPERIMENTAL SETUP.....	5
4.1. Specimen Construction .....	6
4.2. Crack Sensor Installation.....	8
4.3. FRP and VE Application .....	8
4.4. Instrumentation and Data Acquisition .....	10
4.5. Charges .....	12
5. EXPERIMENTAL RESULTS.....	13
5.1. FRP-VE Removal and Other Observations .....	13
5.2. Previous Laboratory Crack Sensor Measurements .....	16
5.3. Sensor Measurements from Blast Tests.....	17
6. CONCLUDING REMARKS.....	25
REFERENCES .....	25
APPENDIX.....	27
A.1 Three-column Specimen Drawings.....	27
A.2 USC_RC Column Analysis Results.....	29

## LIST OF ILLUSTRATIONS

	Page
Figure 2.1. Cut-Away View of Crack Sensor (McDaniel, 2004) .....	2
Figure 2.2. Path of Current along Disturbed Outer Conductor (McDaniel, 2004) .....	2
Figure 2.3. Separation of Steel Spirals in Two Cracks .....	3
Figure 3.1. 3-D Rendering of the Three-Column Specimen.....	4
Figure 4.1. One Layer of Reinforcement for Footing and Slab .....	6
Figure 4.2. Formwork and Reinforcement for Footing.....	6
Figure 4.3. (a) Column Reinforcement and (b) Shoring and Formwork for Slab .....	7
Figure 4.4. Steel Plate to Protect Sensor Connectors.....	8
Figure 4.5. Final Column Specimen before Testing .....	9
Figure 4.6. Accelerometer.....	10
Figure 4.7. Pressure Transducer.....	10
Figure 4.8. Instrumentation Layout .....	11
Figure 4.9. Aluminum Box with DAQ Systems .....	12
Figure 4.10. Test Site .....	12
Figure 4.11. First 4 lbs Charge.....	13
Figure 5.1. Post-Test Inspection on Column 2 .....	14
Figure 5.2. Back Side of Column 3.....	15
Figure 5.3. Comparison of Permanent Deflections.....	16
Figure 5.4. Signals from Sensors in Two FRP-Wrapped Columns (McDaniel, 2004) ....	16
Figure 5.5. Time History of Sensor Signal from a Shake Table Test (Xue, 2006).....	17
Figure 5.6. Dynamic Data from Column 1 during the 2 <sup>nd</sup> 4 lbs Blast .....	18
Figure 5.7. Dynamic Data from Column 1 during the 10 lbs Blast.....	18
Figure 5.8. Tension Strain versus Crack Sensor Measurement at Mid-height .....	20
Figure 5.9. Crack Sensor Signals Taken after the 2 <sup>nd</sup> 4 lb Blast (Differenced with the Signals Taken before the 2 <sup>nd</sup> 4 lb Blast) .....	21
Figure 5.10. Crack Sensor Signals Taken after the 10 lbs Blast (Differenced with the Signals Taken before the 2 <sup>nd</sup> 4 lb Blast) .....	21
Figure 5.11. Crack Sensor Signals Taken after the 10 lbs Blast (Differenced with the Signals Taken before the 10 lb Blast).....	22
Figure 5.12. Crack Sensor Signals Taken after the 30 lb Blast (Differenced with the Signals Taken before the 2 <sup>nd</sup> 4 lb Blast) .....	22
Figure 5.13. Column 1 2 <sup>nd</sup> 4 lbs Crack Sensor Signal Compared to Picture of Cracking	23
Figure 5.14. Column 1 10 lbs Crack Sensor Signal Compared to Picture of Cracking....	24
Figure 5.15. Column 1 30 lbs Crack Sensor Signal Compared to Picture of Cracking....	24
Figure A.1. Column Reinforcement Details .....	27
Figure A.2. Dimensions of Footing and Slab .....	28
Figure A.3. Reinforcement Details for Footing and Slab .....	28
Figure A.4. Stress-Strain Relationship for Concrete .....	29
Figure A.5. Stress-Strain Relationship of Rebar.....	29
Figure A.6. Column Interaction Diagram.....	30
Figure A.7. Moment Curvature Diagram.....	30
Figure A.8. Force-Deflection Diagram for a Point Load at Mid-height.....	31

## **1. INTRODUCTION**

Columns in bridges serve a critically important role in the overall load path of a structural system. In the event of an earthquake or explosion, damage or failure of one or more columns will cause either collapse or redistribution of loads which could ultimately lead to collapse. As such, monitoring and assessing the condition of bridge columns is of paramount importance.

In reinforced concrete (RC) columns, it is often difficult to detect cracks after an earthquake or explosion event is over. Unless the event is catastrophic, gravity loads most likely close the cracks, rendering them visually undetectable. In this case, the coaxial cable crack sensor developed by Chen *et al.* (2004; 2005a; 2005b) can be applied to assist in crack detections during static, cyclic, and dynamic loading with a commercial time-domain reflectometer (TDR). A single cable sensor can provide the damage information along the length of the cable when embedded into a RC column, including both the severity and the location of damage. Cable sensors are cost-effective, rugged, and easy to use for large-scale civil engineering structures. They have a unique ‘memory’ feature, remembering the most severe damage during a significant event. This feature allows engineers to retrieve damage information after the event is over, enhancing the reliability of damage detections with cable sensors.

A commercial TDR can only be used to measure one frame (response to cracks at one time instant) for the complete information along the length of each cable sensor. To enable one measurement of a series of frames, Xue (2006) developed a high-speed TDR system that can be used with cable sensors to detect cracks in real time. This allows the observation of cracks as they open and close. The system has been tested previously under moderately high strain-rate loading in shake table experiments, but had not been tested under extremely high strain-rate loading such as blast effects. If implemented, this system could prove to be a valuable tool for real-time monitoring of structural conditions and for the assessment of post-disaster damage.

This report presents the results from a series of blast tests that took place at the Fort Leonard Wood Army Base in Missouri. The objectives of the testing were to investigate the performance of coaxial cable crack sensors when measured dynamically under high strain-rate loading, and to validate the performance of a novel fiber reinforced polymer (FRP) and visco-elastic (VE) blast retrofitting system for RC columns. This report focuses mainly on the results of the crack sensor testing. Results from previous static and dynamic laboratory testing of the crack sensors are also included for comparison.

## **2. BACKGROUND OF COAXIAL CABLE CRACK SENSORS**

### **2.1. Design and Measurement**

The crack sensors developed by Chen *et al.* (2004; 2005a; 2005b) have undergone extensive testing to understand their behavior under static loading as well as the influence of environmental factors on their performance in field condition. The principle that the

sensor design is based on is called electrical time-domain reflectometry (ETDR). In this case, a cable functions both as a sensor and as a signal carrier. ETDR is a remote sensing technology that implements the use of information collected from the reflected wave along the length of a signal carrier after an electric signal in the form of fast-rising pulses has propagated through the signal carrier (McDaniel, 2004).

Figure 2.1 shows the cut-away view of a crack sensor.

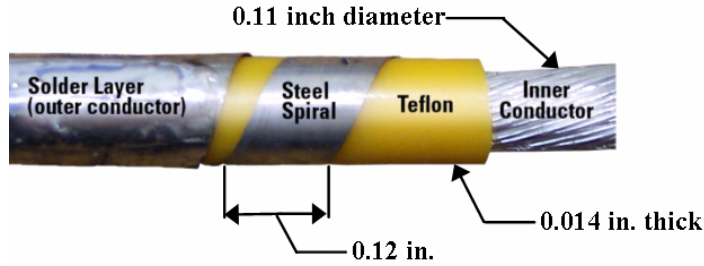


Figure 2.1. Cut-Away View of Crack Sensor (McDaniel, 2004)

To fabricate a cable sensor, a 10 gage wire is wrapped with a stainless steel spiral along the entire length of the cable. A very thin layer of solder is then applied on top of the spirals to create a continuous outer conductor and to prevent premature separation of the spirals. In place of hand-soldering, a thermal spray system that uses plasma gas and a very fine copper powder can be used to create the continuity in the outer conductor. The coating can either be applied using a hand-operated spray gun or by using robotic equipment. Although the robotic equipment creates the most uniform coating, either method (hand or robot operated) has been proven to create a more consistent coating than the hand-soldering method in addition to being less time-consuming.

The sensor is then embedded into concrete by approximately  $\frac{1}{2}$ " deep. The embedment process can be done either by pre-forming or cutting a  $\frac{1}{2}$ " by  $\frac{1}{2}$ " groove along the face of the member that is monitored for cracks. An adhesive primer is then brushed in the groove, the sensor is placed in the groove, and the groove is filled with grout. When the concrete member is loaded and cracks begin to form, the cracks pull apart the steel spirals on the sensor. This action causes a local disruption in the flow of current which affects the characteristic impedance of the sensor at that location. Figure 2.2 illustrates the effect of a separation in the outer conductor on the flow of current. By measuring the signal voltage using a digital oscilloscope, one can obtain the reflected voltage as a function of time along the length of the cable.

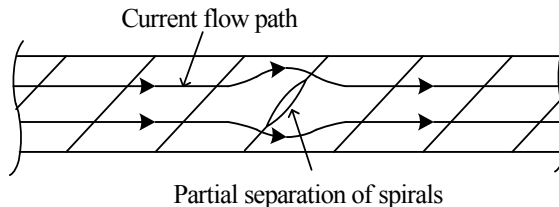


Figure 2.2. Path of Current along Disturbed Outer Conductor (McDaniel, 2004)

The propagation time scale can be converted to distance along the cable by dividing by two and multiplying by the signal propagation velocity, which is based on the electrical properties of the cable. The reflected voltage can be converted to a dimensionless measure called reflection coefficient ( $\rho$ ) by dividing it by the voltage of the original pulse signal. Once these conversions are made, the signal is then in the form of reflection coefficient as a function of distance along the cable. From this data, the locations of various cracks along the member are easily established. Figure 2.3 demonstrates how the sensors work in an actual structure. As can be clearly observed in Figure 2.3, the spirals of the cable were separated around two cracks. Note that cracks do not have to be as large as the ones shown in Figure 2.3 for the sensor to work properly. Past tests indicated that a crack width of as small as 0.005" can be detected by cable sensors (Chen *et al.*, 2004) and two cracks of 1" apart can both be clearly identified from one sensor measurement.



Figure 2.3. Separation of Steel Spirals in Two Cracks

## 2.2. Use for Dynamic Measurement

The new TDR system developed by Xue (2006) is capable of monitoring the signal along the cable sensor in real time under dynamic loading. The system is based on a fast-rising pulse generator and a high-speed digital oscilloscope that performs fast measurement and data storage, thereby allowing real-time measurement and analysis.

This new system allowed a much broader application of the crack sensor technology. It allows the engineer to monitor, in real-time, the opening and closing of

cracks while a dynamic event is occurring. This has important implications for post-disaster assessments since, following a dynamic event, gravity loads will often close cracks that may have formed on a column during the event. During the development of this system, lab experiments were conducted to validate the performance of the sensors under earthquake loading, but no extremely high strain-rate loading, such as blast loading, was conducted.

### 3. SPECIMEN DESIGN

As mentioned previously, one of the objectives of this study was to investigate the hardening effect of a new retrofitting strategy with FRP strengthening and VE damping. To have a fair comparison among two hardening methods, three identical RC columns were cast and tested, including one control column.

#### 3.1. Three-Column Specimen

In order to create three identical columns (before strengthening), a three-column specimen was designed, as shown in Figure 3.1. Each column was designed as a 1/4-scale specimen of a prototype bridge column in Missouri.



Figure 3.1. 3-D Rendering of the Three-Column Specimen

Each column was 8 feet long and 10 inches in diameter; it was reinforced with 6 #3 deformed bars and #3 hoops every 6". All reinforcement was Grade 60, and the reinforcement and detailing was designed based on the provisions of ACI 318-02 (2002). The specimen had a 12" thick footing and a 12" thick slab on top. The purpose of the three-column layout is such that the explosive charge may be suspended from the top of the specimen so as to induce an identical blast load on each of the three columns. The top slab was also balanced over the three columns so that very little end moment would

be present on the columns before they were loaded by the blast pressure. Column 1 was the control specimen and had no strengthening. Column 2 was strengthened with one layer of carbon FRP for confinement, and Column 3 was strengthened with the FRP-VE system. Detailed drawings of the specimen design can be found in Figures A.1 – A.3 in Appendix A.1.

### **3.2. Capacity Analysis**

The computer program USC\_RC, developed by Dr. Asad Esmaily at the University of Southern California, was used to determine the capacity of Column 1. The model takes into account the confinement provided by the ties by utilizing the Mander Confinement Model (Esmaily, 2001). Even though the spacing of the ties is relatively large (6”), they still provide some ductility enhancement with little increase in strength as shown in Figure A.4 in Appendix A.2. The column model also takes into account strain-rate effects indirectly by inputting dynamic increase factors (DIF’s). The DIF’s used for this analysis came from the Technical Manual TM 5-1300 (Joint Departments of the Army, the Navy, and the Air Force, 1990), and are based on flexure for the close-in design range. The factors used are likely to be lower than the actual DIF’s for the impulsive type loading seen in these experiments, but it is difficult to determine a definite strain rate from the experimental data that was obtained. The input parameters are included in Appendix A.2.

Moment-Axial Force Interaction and Moment-Curvature for a constant axial force of 1.84 kips (weight of slab) diagrams were developed with USC\_RC for the column. The analysis was set to terminate when either the confined concrete exceeded the ultimate strain or the steel strain exceeded the rupture value. In this case, the confined concrete exceeded its ultimate strain much before the steel ruptured. The Moment-Curvature analysis yielded a maximum moment capacity of 18.7 k-ft and a curvature ductility ratio of 29 (at a maximum curvature of  $9.49 \times 10^{-3} \text{ in}^{-1}$ ). A Force-Displacement diagram for a point load at the mid-height of the column was also developed. This yielded a lateral load capacity of 9.3 kips and a lateral displacement capacity of 2.4 inches (at mid-height). These diagrams are presented in Appendix A.2.

## **4. CONSTRUCTION AND EXPERIMENTAL SETUP**

Due to the size of both the test specimen and the explosive charge, the blast test was conducted at one of the blast ranges at Fort Leonard Wood Army Base. The specimen was constructed and cured in the High Bay Structures Lab at the Missouri University of Science and Technology (Missouri S&T) and then transported to the test site at Fort Leonard Wood. After the specimen was situated at the test site, coaxial cable crack sensors were first installed in each column, the FRP and VE retrofits were then applied, and all the instrumentation was finally set up.

#### 4.1. Specimen Construction

The steel cages that would be placed in the footing and top slab were constructed as shown in Figure 4.1. Each had reinforcement in the top and bottom, and all reinforcement was designed to be symmetrical about the central axis. The member dimensions, rebar sizes and details can be found in Appendix A.1.

Once each layer of reinforcement was tied together, they were placed in the forms, and the reinforcement for the column-footing construction joints were tied in place as shown in Figure 4.2. As shown in the figure, standard 90° hooks detailed using ACI 318-02 (2002) were utilized at these joints.



Figure 4.1. One Layer of Reinforcement for Footing and Slab

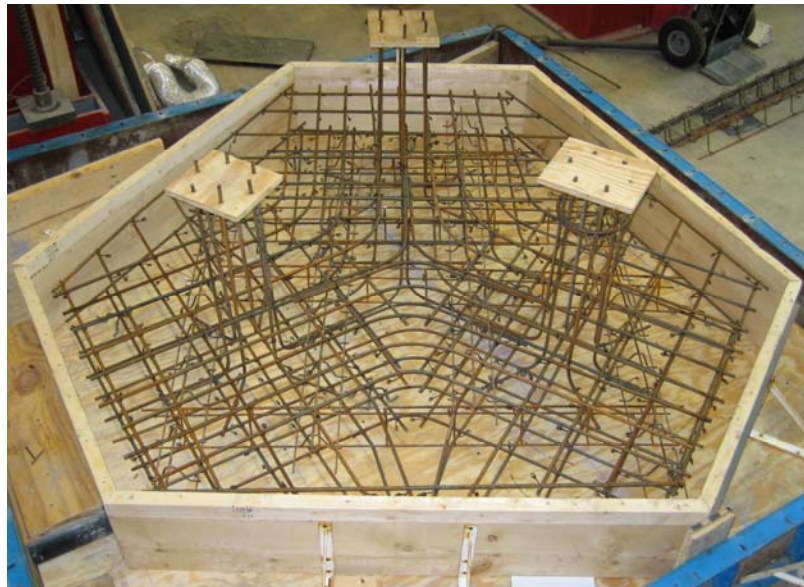


Figure 4.2. Formwork and Reinforcement for Footing

The reinforcement for the columns was tied separately and then attached to the dowel bars that were extended out from the footing. On each column reinforcement cage, six strain gages were attached at the points of maximum positive and negative moment. Since the reinforcement was spliced at the bottom joint, strain gages for negative moment were placed at the top of the column. Two gages were used for positive moment (one for tension and one for compression), and four were used for negative moment in the same fashion. Only two of the gages at the top of the column would be used, but four were applied for redundancy in case any of the gages were damaged during the pouring of the concrete.

Once the column reinforcement was in place, the top slab was completed much in the same fashion as the footing, and a pipe was placed in the center of the slab so that the charges could be suspended from the top. Since the slab was only 12" thick, the longitudinal column reinforcement had to be bent into 90° hooks to ensure proper development length. Figure 4.3 (a) and (b) show the in-place column reinforcement before placing the forms, and the shoring and formwork for the slab, respectively.



(a)



(b)

Figure 4.3. (a) Column Reinforcement and (b) Shoring and Formwork for Slab

During both concrete pours, six 4" cylinders were prepared in order to verify the concrete compressive strength. One was tested at 7 days, one at 21 days, and four at 28 days. The 28-day compressive strengths of the footing and column/slab concrete, respectively, were 4.8 ksi and 5.3 ksi. The reason for the difference in compressive

strengths (besides being different batches of concrete) was that too much water was added to the footing concrete before pouring to make it more workable.

#### **4.2. Crack Sensor Installation**

Each column had one coaxial cable crack sensor embedded on its back side (tension face). Normally, the sensor's connector would extend out of the base of the column. In this case, to protect the connector from the blast, the cable was bent at the base of the column and embedded in the top of the footing as well. To do this, a ½" by ½" groove was cut along the back of the column and in the footing that extended all the way to the edge of the footing. The sensor was then placed in the groove and grouted using Carter Waters CW100 Precision Grout that was mixed to a dry-pack consistency. Following the first blast, a large portion of the grout was separated from the column groove due partly to the tension reflected wave generated at the back side of the column under explosion. The main reason was that since the grout was mixed to a dry-pack consistency, it did not have a sufficiently high water content to create a good bond to the base concrete. To solve this problem, all subsequent grout repairs were done by first brushing Sikatop Plus Component A bonding agent into the groove before packing the grout. This significantly improved the bond between the grout and the concrete. Finally, to protect the sensors' connectors from the blast pressure and debris, steel plates were fabricated and attached to the footing as shown in Figure 4.4.



Figure 4.4. Steel Plate to Protect Sensor Connectors

#### **4.3. FRP and VE Application**

Column 1 was designated as the control column and had no strengthening, but it was painted white in order to see the cracking more clearly. Column 2 was strengthened with one layer of carbon FRP for confinement, and Column 3 was strengthened with the FRP-VE system. In addition to one layer of carbon FRP, one VE layer was applied to Column 3.

On Column 2, the carbon FRP was wrapped around the column and encapsulated in Wabo MBrace Saturant Epoxy Encapsulation Resin. The saturant comes in two parts

which are mixed just before using. One layer is applied to the concrete before applying the fabric using a nap roller, and then another layer is applied on top of the fabric so that the FRP is completely encapsulated by the saturant. To ensure proper confinement, the fabric was overlapped on the back side of the column by 6 inches.

On Column 3, the first layer of carbon FRP was applied in the same manner as Column 2. Once the saturant began to harden, the VE material was applied on top and another layer of saturant was brushed onto the VE material. The final layer of carbon FRP was then applied on top of the VE material in the same manner as the first, except that the fibers were oriented along the length of the column. Figure 4.5 shows the column specimen after strengthening and sensor installation.

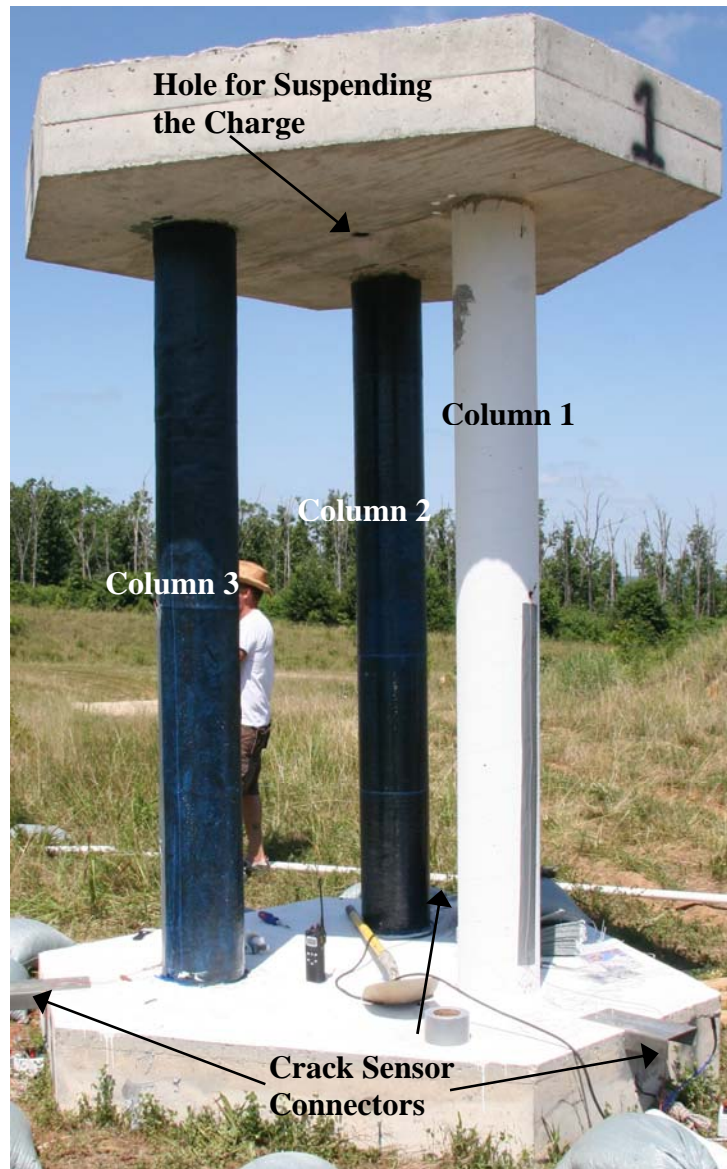


Figure 4.5. Final Column Specimen before Testing

#### 4.4. Instrumentation and Data Acquisition

In addition to the crack sensors and the strain gages, each column was instrumented with one accelerometer. The accelerometers were attached by gluing a mounting clip to the back side of each column at mid-height. On Columns 1 and 2, the clip was glued directly to the concrete and FRP wrap, respectively. On Column 3, a small hole was cut in the outer FRP and VE material so that the clip could be glued to the first layer of FRP. This was done to obtain the acceleration of the column itself and to avoid a false acceleration from the much less stiff VE material. Figure 4.6 shows one of the accelerometers ready for measurement.



Figure 4.6. Accelerometer

Three pressure transducers were also used to verify the blast pressures calculated by various computer programs. They were placed 18 feet from the center of the charge and were pointed directly towards it. This distance was selected based on the measurement range of the transducers and the maximum pressure that they would see during the largest blast. Each transducer was mounted in a pipe, embedded in the ground, and covered with a sandbag to ensure no movement occurred. Figure 4.7 shows one of the pressure transducers. Finally, a video camera was placed at a safe distance on top of a berm to record each blast.



Figure 4.7. Pressure Transducer

Several different systems were utilized for data acquisition. To acquire the strain and pressure data, a Synergy data recorder at very high sampling rates was used for the blast testing. For the accelerometers, a 'Black Box' data recorder was used. A sampling rate of 20 kHz was used for both the Synergy and 'Black Box' data recorders. For the crack sensors, a Digital TDR Oscilloscope was used along with a pulse generator which is used for dynamic measurements. The Oscilloscope only has one channel, so dynamic measurements were only taken from Column 1, but static measurements were taken on each column both before and after each blast. A laptop was also used to configure and record data from the Synergy and 'Black Box' data recorders. Finally, to protect all of the data acquisition systems from the blast, everything was placed in an aluminum box. The box was situated in a ditch next to the column specimen and covered with 6 x 6 timbers which were covered with plywood and sandbags. All of the cabling for the transducers was piped through PVC pipes which were secured with sandbags. Figure 4.8 and Figure 4.9 show the layout of the instrumentation and the aluminum box containing all of the data acquisition systems, respectively, and Figure 4.10 is a picture of the test site.

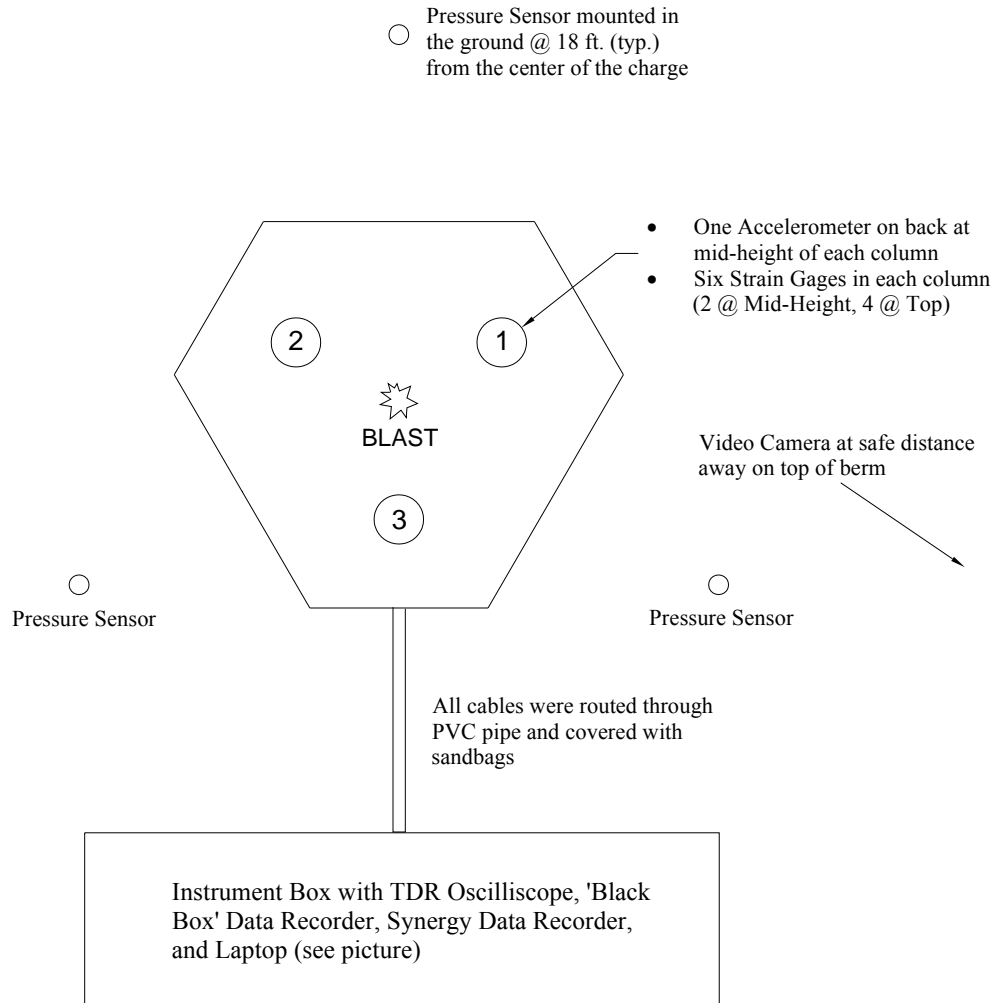


Figure 4.8. Instrumentation Layout

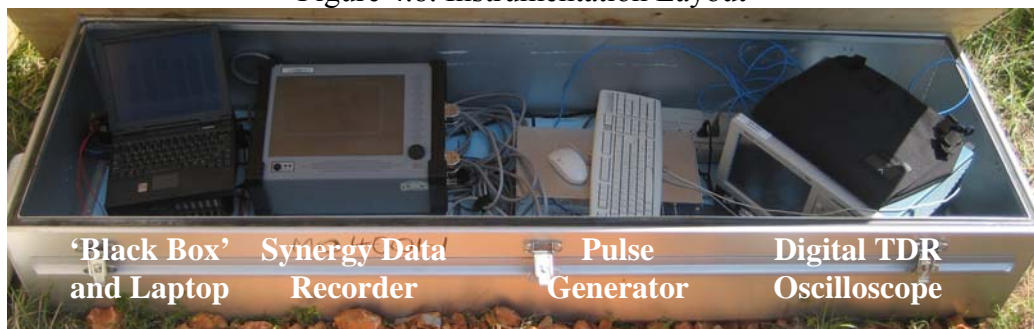


Figure 4.9. Aluminum Box with DAQ Systems



Figure 4.10. Test Site

#### 4.5. Charges

Four different charges were used for the testing. Charge weight is always specified in TNT (Trinitrotoluene) equivalence. The TNT equivalence factor is defined as the ratio of the mass specific energy of the explosive compound to the mass specific energy of TNT (4520 kJ/kg). An alternative approach makes use of two conversion factors, depending on whether the peak overpressure or impulse is to be matched (Mays and Smith, 1995).

The first two charges were made up of pentolite cast boosters, each having a TNT equivalence of 1.1, for a total charge weight of 4.4 lbs of TNT (hereafter referred to as the 4 lbs blasts). The third charge was made up of nine pentolite cast boosters and a 0.25 lbs pentolite cast booster, for a total charge weight of 10.2 lbs of TNT (hereafter referred to as the 10 lb blast). The fourth charge was made up of ammonium nitrate fuel oil (ANFO), with a TNT equivalence of 0.83, along with 2 pentolite cast boosters for a total charge weight of 30 lbs of TNT.

The first charge was placed on a piece of plywood which was sitting on a cardboard Sonotube, as shown in Figure 4.11. When inspecting the columns after the first blast, it was determined that the plywood had caused some of the damage to Column 3. While debris damage would be a normal occurrence during a blast, it is difficult to predict and was not considered in this research. Therefore, the second 4 lbs charge and

the 10 lbs charge were suspended from the top slab. The ANFO used for the 30 lbs charge was put in a bag and placed on top of a cardboard Sonotube (with no plywood).



Figure 4.11. First 4 lbs Charge

## 5. EXPERIMENTAL RESULTS

After the completion of each blast, a thorough inspection of each column was performed. Crack patterns were observed, and the damage to each column and its respective strengthening system was assessed. Crack sensor measurements were taken both before and after each blast, along with dynamic measurements on Column 1. It should be noted that on the two columns that were strengthened, cracks cannot be observed visually. For these columns, the coaxial cable crack sensors were used to locate cracks after each blast.

### 5.1. FRP-VE Removal and Other Observations

Following the completion of the 30 lbs blast, some of the FRP and VE materials were removed from Columns 2 and 3. This allowed a thorough inspection of the condition of the concrete underneath the strengthening materials and exposed any cracks that may have formed which would otherwise have only been detected by the crack sensors.

Removal of the FRP from Column 2 led to some interesting findings. Most cracks were located at the failure hinge. At the base of the column, one large crack was present on the tension side as seen in Figure 5.1 (a), but no other cracking was visible. The FRP was not removed at the top of the member, but it is expected that similar cracking occurred at that location since the loading was symmetric and the boundary conditions at the joint were the same as those at the base (except for the splice in the flexural reinforcement at the base). There were several separated cracks at the mid-height of the column as seen in Figure 5.1 (b), but they were all flexural cracks, and there were no diagonal or horizontal cracks connected together like those seen on the control column. Other than on the front face of the column at the mid-height, all of the concrete was intact, and there was no sign of loose material. This indicates that the FRP protected the concrete from spalling and from further cracking such as that seen on Column 1.



(a) Crack at Base



(b) Hinge at Mid-Height

Figure 5.1. Post-Test Inspection on Column 2

Removal of the FRP and VE materials from Column 3 led to similar findings. Most of the outer FRP and VE material along the column was removed, but only the inner layer of FRP that was around the failure hinge was removable because of its bond to the concrete. There was a small amount of spalling on the front of the column, but not enough to expose the reinforcement. The crack pattern on the back side of the failure hinge was similar to that of Column 2, but the cracks as shown in Figure 5.2 were narrower.



Figure 5.2. Back Side of Column 3

As noted previously, the 30 lbs blast resulted in flexural failure of all three columns by creating a hinge at the mid-height of each member. It was noticed, however, that Column 3 did not have as much permanent deflection as Columns 1 and 2. Since it is very difficult to measure this deflection in the field, pictures were taken of each column and the deflection was estimated. Figure 5.3 shows a comparison of the three columns and their respective deflections following the 30 lbs. blast.

It can be seen from Figure 5.3 that after the blast, Column 3 had 50% less permanent deflection than the other two columns. This means that a significant amount of the energy generated by the blast was dissipated. Columns 2 and 3 both had a layer of FRP designed to confine the concrete. This confining action increases the ductility of the section, thereby dissipating energy when significant inelastic deformations are present. However, since Columns 2 and 3 had the same confinement FRP layer, and Columns 1 and 2 had approximately the same amount of permanent deflection, this additional energy dissipation could only be explained by the addition of the VE material. This alone provides evidence that this FRP-VE strengthening system adds a significant amount of damping as well as ductility to a reinforced concrete section.



Figure 5.3. Comparison of Permanent Deflections

## 5.2. Previous Laboratory Crack Sensor Measurements

A number of tests were conducted in the Highbay Structures Laboratory at Missouri S&T. Figure 5.4 shows the signals from the shake table tests on two columns that have been wrapped with FRP (McDaniel, 2004).

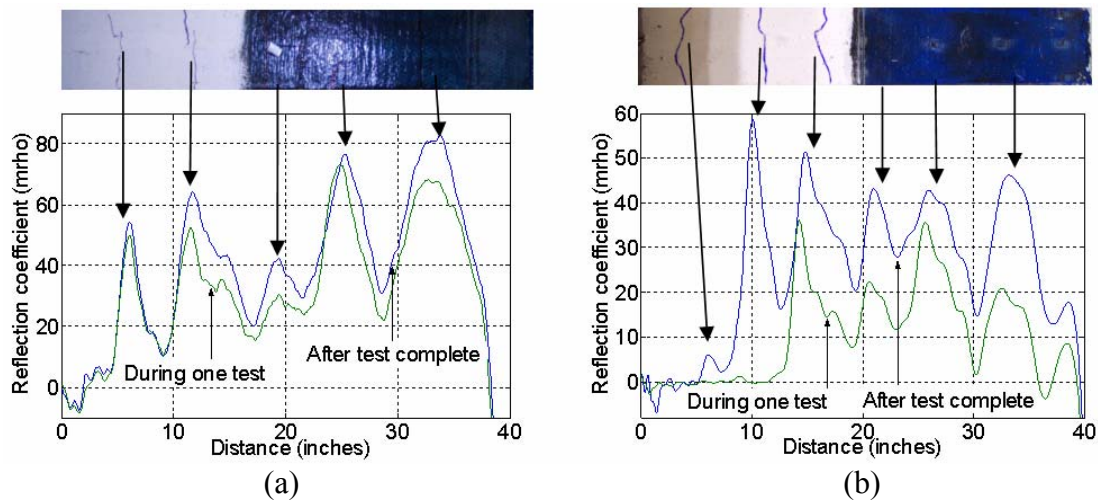


Figure 5.4. Signals from Sensors in Two FRP-Wrapped Columns (McDaniel, 2004)

The figures demonstrate the successful application of the sensors in detecting cracks that are not visible due to a retrofitting system. They also demonstrate the memory feature of the sensors. The signals shown in blue were taken after the load had been removed from the columns and the cracks had closed due to gravity loads. The reflection coefficient measured indicated the presence of multiple cracks during the past shaking. It correlated well with one of the reflection coefficient curve taken during the shaking test.

After Xue (2006) developed the dynamic testing equipment, it was possible to record data in real-time, such as that shown in Figure 5.5. The figure shows 14 seconds of data from a sensor embedded in a column. The column was tested on a shake table with an earthquake record input.

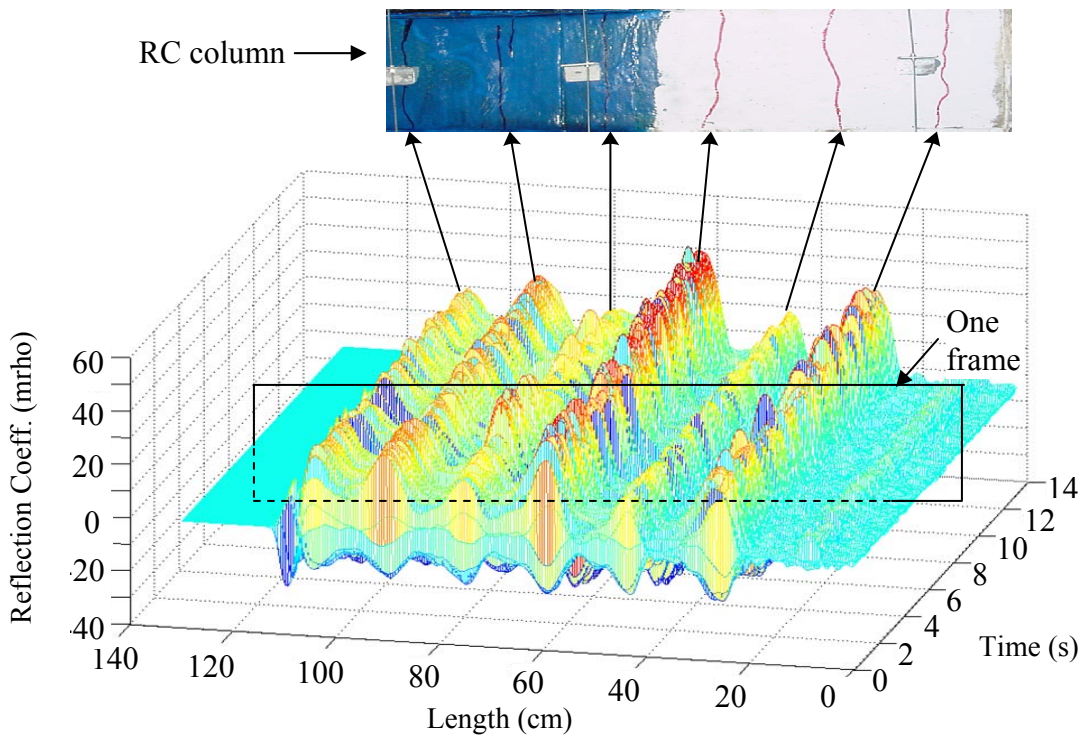


Figure 5.5. Time History of Sensor Signal from a Shake Table Test (Xue, 2006)

### 5.3. Sensor Measurements from Blast Tests

The crack sensors were used to record dynamic data from Column 1 during the blasts and to record static data both before and after each blast. The sensors were embedded in the footing of the columns as well, but since the footing had minimal cracking from the blast, only the column portion of the sensor data is presented.

One of the main objectives of this research was to validate the performance of these sensors under a high strain-rate event, such as a blast. The sensors worked well during the dynamic testing. In fact, the crack sensors supplied more data than many of the other transducers used in the testing. It was shown that it is possible to record

cracking during a loading event. One ‘frame’ of dynamic data was captured every 0.5 msec, which should be fast enough to capture the response of the column to the impulsive load since its natural period is approximately 18 msec. For clarity, ‘snapshots’ of certain frames of data were taken from the dynamic data and plotted to show the progression of cracking during the blast. Figure 5.6 shows dynamic data from the second 4 lbs blast and Figure 5.7 shows data from the 10 lbs blast. Dynamic data was not recorded for either the first 4 lbs blast or the 30 lbs blast.

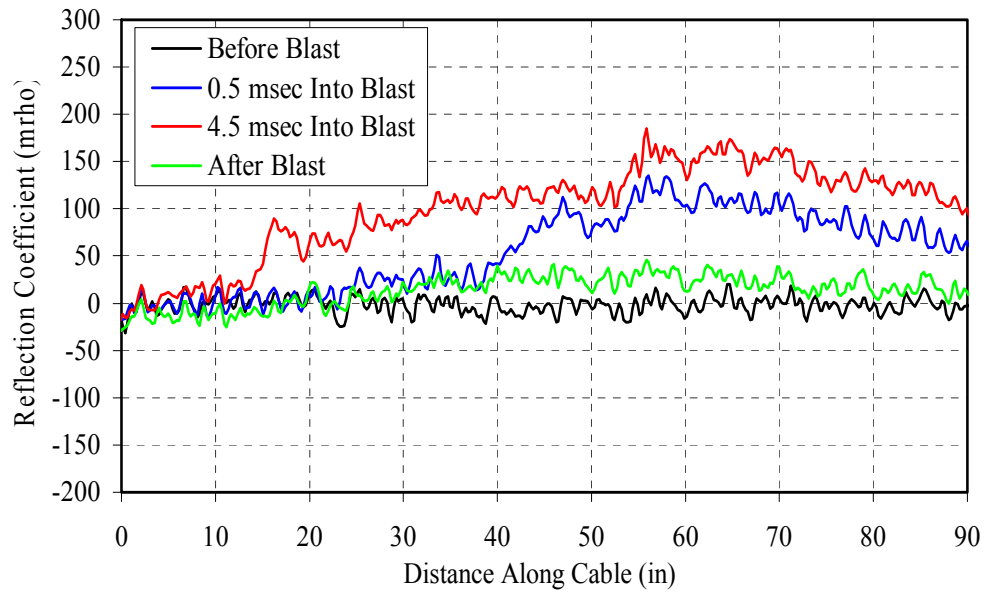


Figure 5.6. Dynamic Data from Column 1 during the 2<sup>nd</sup> 4 lbs Blast

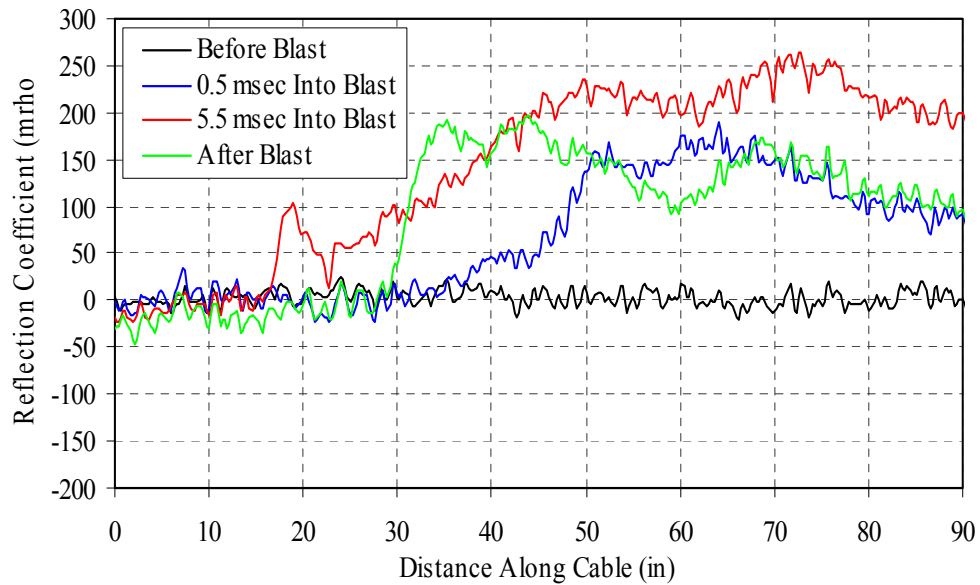


Figure 5.7. Dynamic Data from Column 1 during the 10 lbs Blast

Figure 5.6 shows that the reflection coefficient generally increases, then decreases, and finally approaches to its near original position. The 4 lbs blasts did not create severe damage to Column 1, but they did cause significant cracking around the mid-height. The green line in Figure 5.6 shows how this cracking affected the final signal along the sensor, as the signal was slightly off its original position. Similar trend has been observed in Figure 5.7 in a much more pronounced manner, as the 10 lbs blast caused significant spalling on the back of the column where the sensor was embedded. This phenomenon was investigated before and typically referred to as “memory” feature (Chen *et al.*, 2005b).

In comparison with Figure 5.4, the local peaks in Figures 5.6 and 5.7 are not clearly seen due to the limited spatial resolution with the old design of the TDR. In the blast test, each sensor is approximately 8 feet long with a connection cable of over 20 feet. Both are much longer than those used in the shake table tests (Chen *et al.*, 2005b). In other words, there was approximately 1/4" between individual data points along the sensor. This resolution is too coarse to see individual peaks, but fine enough to see the overall response. For very high sampling rates, large amounts of data are generated and must be stored. The data acquisition system that was used in the blast testing had limited storage space, thus limiting the resolution that could be used while still sampling fast enough to capture the column's response to the blast. This issue will be resolved completely in a new DAQ system that is currently under development. The new system will save data to an external location, thus allowing virtually unlimited data storage.

To relate strain to the crack sensor signal, a comparison was made relating the strain at the mid-height of the column to the crack sensor reflection coefficient at that location. Since the strain gage on the back side of the column (positive moment – tension) was at the same location as the crack sensor, this gage was used for comparison. The reflection coefficient at the mid-height of the column was extracted from each frame of dynamic data from the 4 lbs blast. Figure 5.8 shows this comparison. It is very clear that the shape of the strain response is similar to the shape of the crack sensor response. This is an anticipated yet interesting result since the width of cracks is directly related to the strain distribution across the member. It would be desirable to proceed with more testing in this area since one set of data is insufficient to make a tangible conclusion or an empirical correlation.

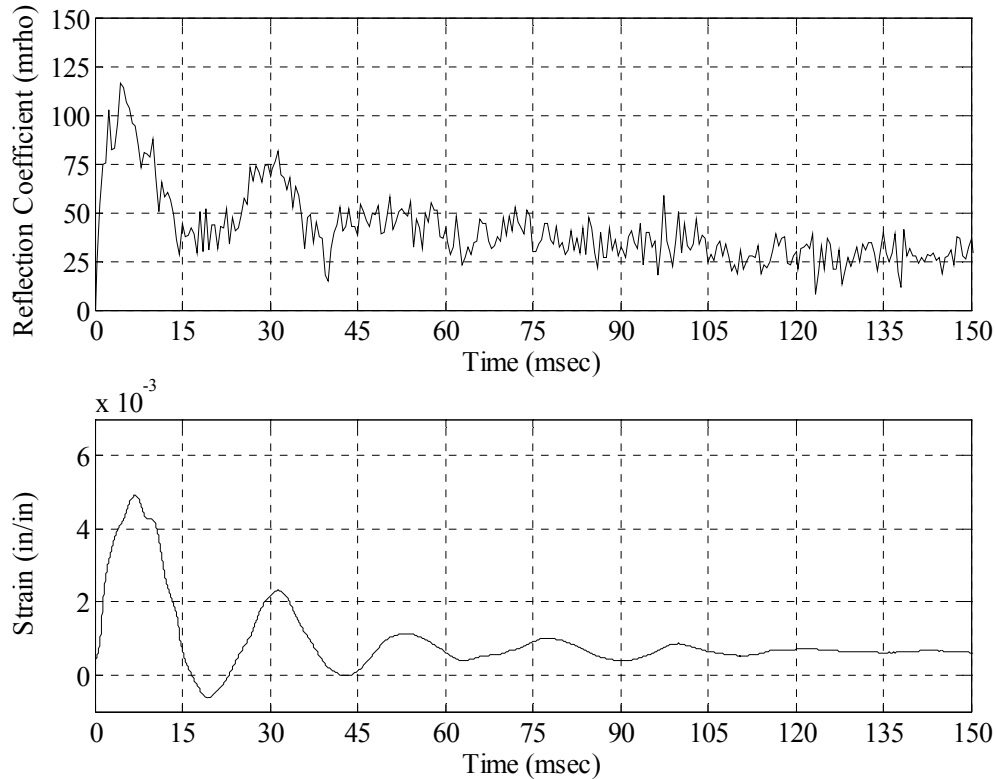


Figure 5.8. Tension Strain versus Crack Sensor Measurement at Mid-height

Static measurements were taken from the crack sensors embedded in all three columns at the following times: before and after the 2nd 4 lbs blast, before and after the 10 lbs blast, and after the 30 lbs blast. Due to equipment problems after the first blast, static measurements were not obtained from the first 4 lbs blast. Comparisons of the three columns and their corresponding crack sensor signals are shown in Figure 5.9 through Figure 5.12.

As can be seen in Figure 5.9, the blast did not cause severe cracking, and Column 1 was subjected to more cracking than Columns 2 and 3. As shown in Figure 5.10 and Figure 5.11, the 10 lbs blast caused much more cracking in Column 1 than the 4 lbs blast, but Columns 2 and 3 still had low levels of cracking. The only difference in the two figures is that Figure 5.10 is differenced with the signals taken before the 4 lbs blast while Figure 5.11 is differenced with the signals taken before the 10 lbs blast. In other words, Figure 5.10 shows the cracking caused from both the 4 lbs and 10 lbs blasts while Figure 5.11 only shows the cracking caused from the 10 lbs blast. This is why the blue curve in Figure 5.10 has higher amplitudes than the blue curve in Figure 5.11.

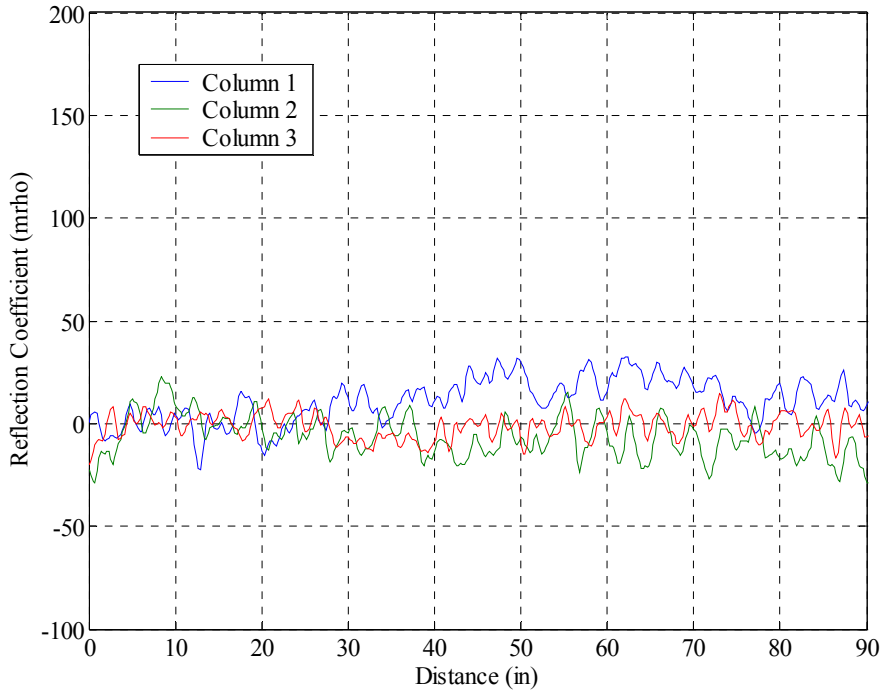


Figure 5.9. Crack Sensor Signals Taken after the 2<sup>nd</sup> 4 lb Blast (Differenced with the Signals Taken before the 2<sup>nd</sup> 4 lb Blast)

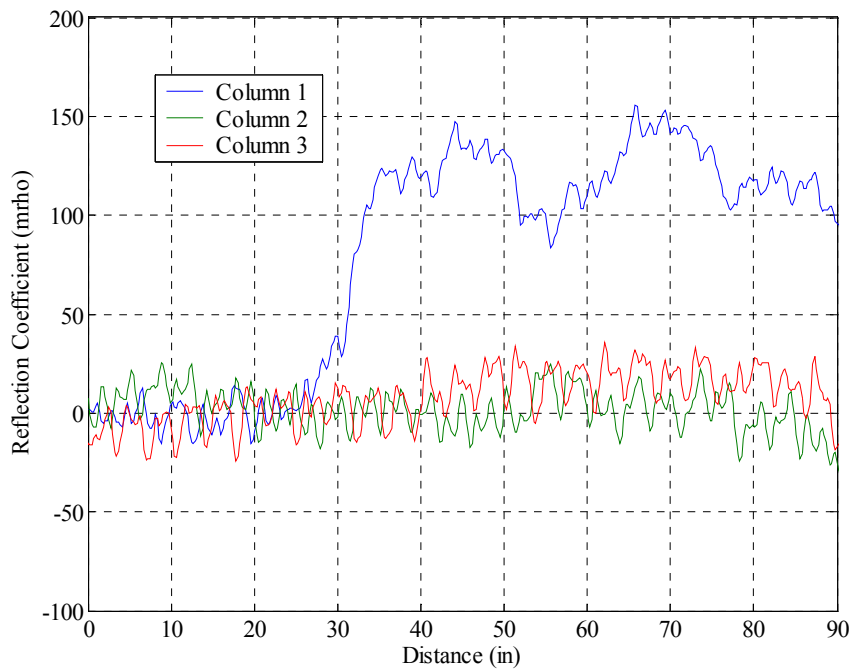


Figure 5.10. Crack Sensor Signals Taken after the 10 lbs Blast (Differenced with the Signals Taken before the 2<sup>nd</sup> 4 lb Blast)

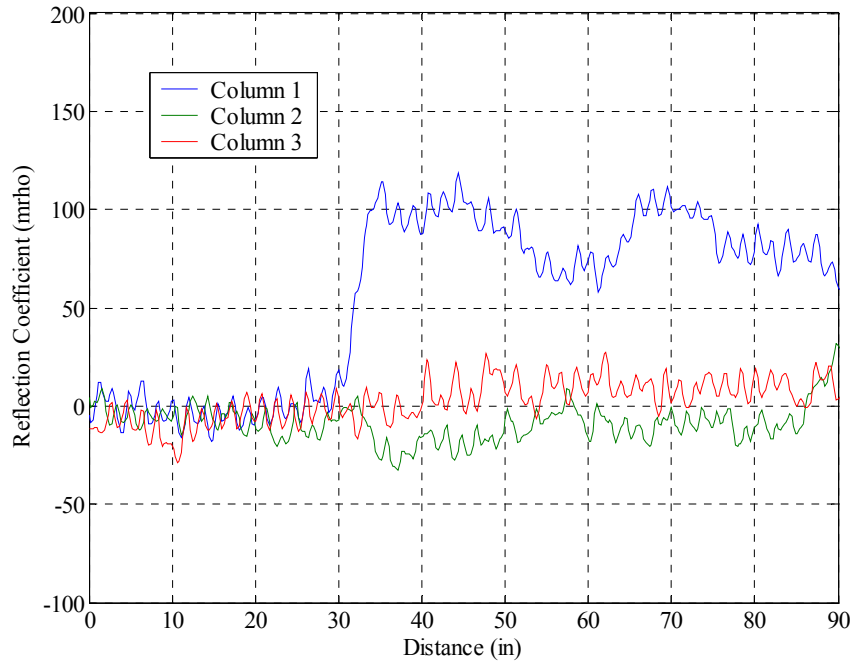


Figure 5.11. Crack Sensor Signals Taken after the 10 lbs Blast (Differenced with the Signals Taken before the 10 lb Blast)

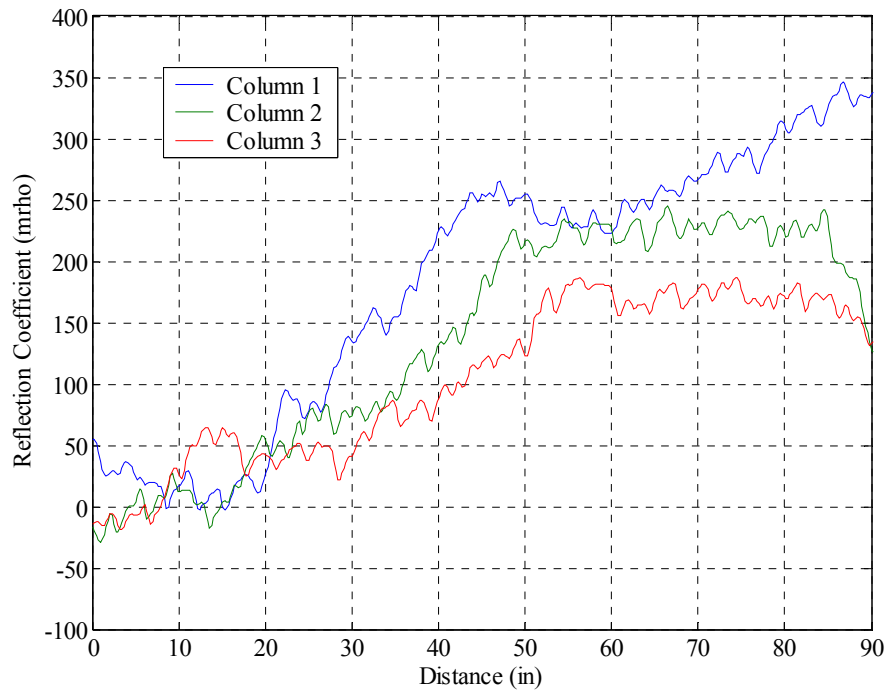


Figure 5.12. Crack Sensor Signals Taken after the 30 lb Blast (Differenced with the Signals Taken before the 2<sup>nd</sup> 4 lb Blast)

Figure 5.12 shows the severity of cracking that occurred from the 30 lbs blast, which failed all three columns. It does, however, show that there was a reduction in cracking from Column 1 to Columns 2 and 3. For each column, a sudden change in reflection coefficient can be observed around mid-height. This change is attributable to the formation of a plastic hinge at the mid-height of the column.

Column 1 was unstrengthened, allowing for visual inspection of cracking after each blast test. Figure 5.13 shows the reflection coefficient due to the 2<sup>nd</sup> 4 lb blast. The blue lines in the picture designate the cracks that occurred from the 1<sup>st</sup> 4 lb blast, and the red lines indicate the cracks that occurred from the 2<sup>nd</sup> 4 lb blast. It seems difficult to distinguish individual cracks in the signal. This could be due to the spatial resolution used to record the signal (distance between each data point). It can be seen, however, that the curve starts to increase around the mid-height of the column, where many cracks are located. This trend is also seen in Figure 5.14 and Figure 5.15.

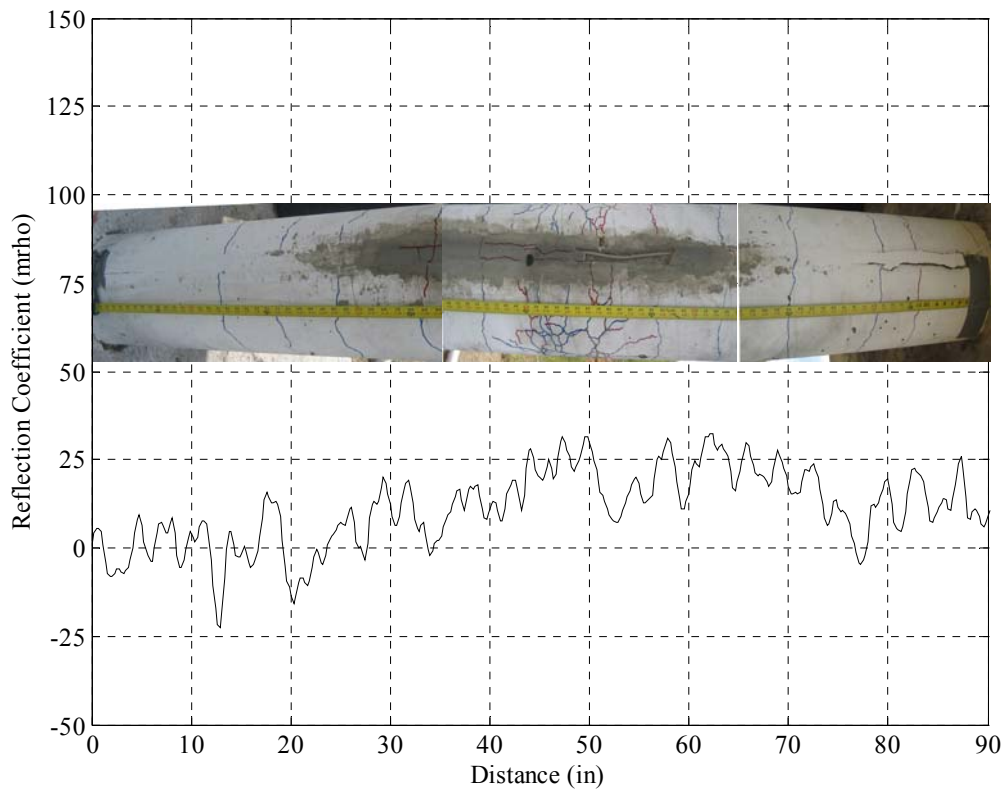


Figure 5.13. Column 1 2<sup>nd</sup> 4 lbs Crack Sensor Signal Compared to Picture of Cracking

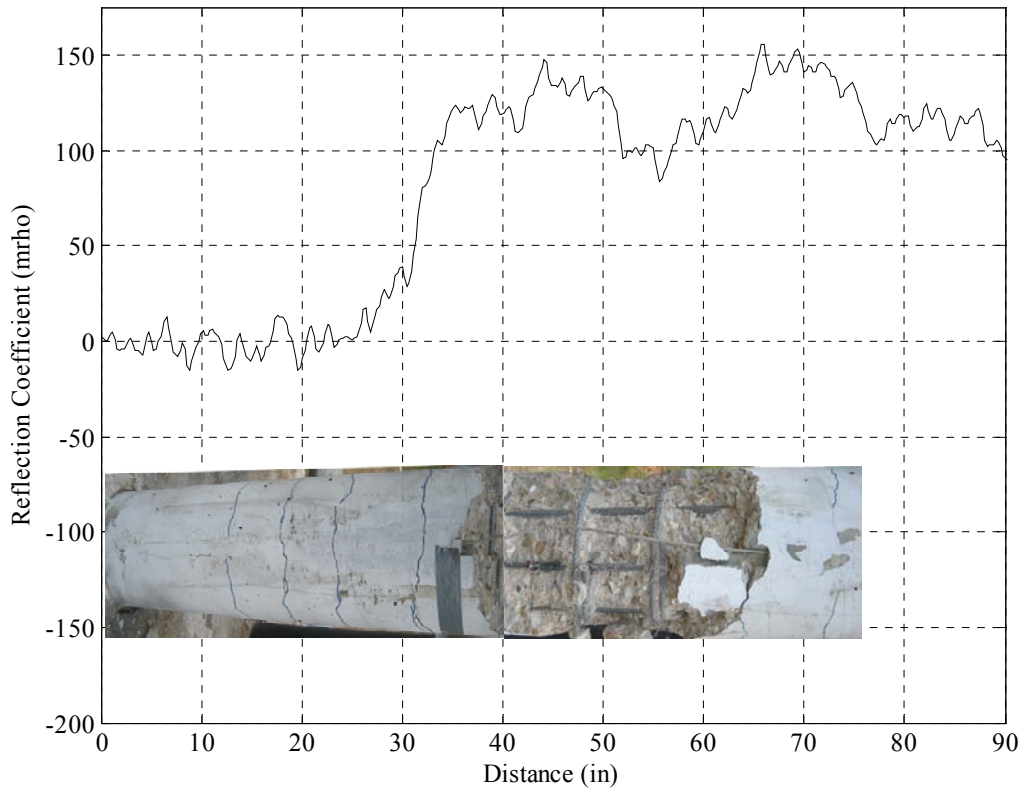


Figure 5.14. Column 1 10 lbs Crack Sensor Signal Compared to Picture of Cracking

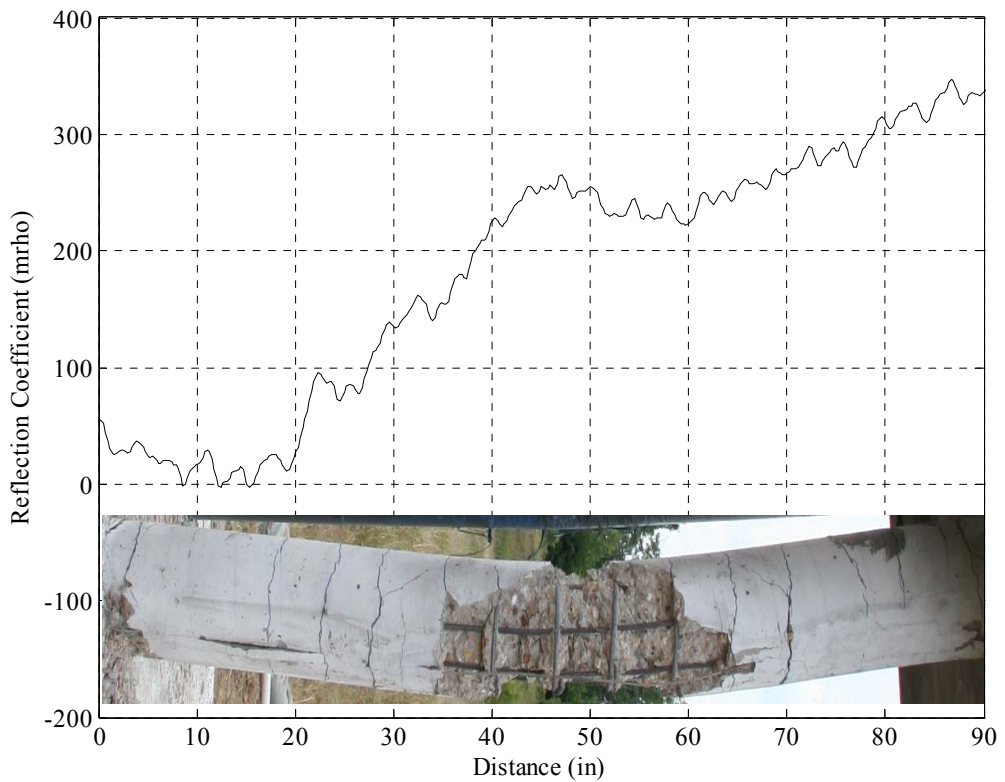


Figure 5.15. Column 1 30 lbs Crack Sensor Signal Compared to Picture of Cracking

## 6. CONCLUDING REMARKS

This study represented the first investigation on the performance of coaxial cable sensors in dynamic measurements under high strain rate loading. Based on the blast test results of three columns, the coaxial cable sensors with the old design of the customized TDR system can dynamically detect the general trend of cracking along the length of each column. When comparing the sensor signals both during and after the blast, the strengthening system showed a significant reduction in cracking when compared to the control column. The reflection coefficient measured from a cable sensor generally correlated well with strains at the nearby location of the column. However, unlike the shake table test results, the local peaks of the sensor signals were not clearly observed due to limited spatial resolutions for this particular application. Currently, a new TDR measurement instrument is being developed for dynamic testing of the crack sensors. When this instrument is completed, better data acquisition will be available for use in future testing.

This study was primarily a proof-of-concept test. Additional tests need to be done in order to further characterize the coaxial cable crack sensors when used to detect cracks at very high loading rates. Future work is directed to:

- Further correlate the dynamic measurements from crack sensors and strain gages,
- Test the new TDR instrument with cable sensors for better understanding of their behavior under dynamic loading.

## REFERENCES

- ACI 318-02 (2002). *Building Code Requirements for Structural Concrete and Commentary*, Committee 318, American Concrete Institute, Farmington Hills, Michigan.
- Chen, G.D., Mu, H.M., Pommerenke, D., and Drewniak, J.L., (2004). "Damage Detection of Reinforced Concrete Beams with Novel Distributed Crack/strain Sensors." *Journal of Structural Health Monitoring*, Vol. 3, No. 3, 225-243.
- Chen, G.D., Sun, S.S., Pommerenke, D., Drewniak, J.L., Greene, G.G., McDaniel, R.D., Belarbi, A., and Mu, H.M., (2005a). "Crack Detection of a Full-Scale Reinforced Concrete Girder with a Distributed Cable Sensor," *Smart Materials and Structures*, Vol.14, No. 3, pp.S88-S97.
- Chen, G.D., McDaniel, R.D., Sun, S.S., Pommerenke, D., and Drewniak, J.L., (2005b). "Distributed Crack Sensors Featuring Unique Memory Capability for Post-Earthquake Condition Assessment of RC Structures," *Journal of Smart Structures and Systems*, Vol.1, No.2, 141-158.
- Esmaily, A., (2001). *USC\_RC Computer Software Help Documents*. Los Angeles, California.
- Joint Departments of the Army, the Navy, and the Air Force. (1990). *Structures to Resist the Effects of Accidental Explosions (TM 5-1300)*. Technical Manual, Washington, DC.

- Mays, G.C. and Smith P.D., (1995). *Blast Effects on Buildings*. London: Thomas Telford Publications.
- McDaniel, R.D., (2004). *Characterization and Implementation of Distributed Coaxial Cable Crack Sensors for Embedment in Reinforced Concrete Structural Members*. M.S. Thesis, University of Missouri – Rolla.
- Xue, L., (2006). *Power Distribution Network Modeling for Design and High-speed Time-domain Reflectometer System Design for Cable Sensor Defect Measurement*. M.S. Thesis, University of Missouri – Rolla.

# APPENDIX

## A.1 Three-column Specimen Drawings

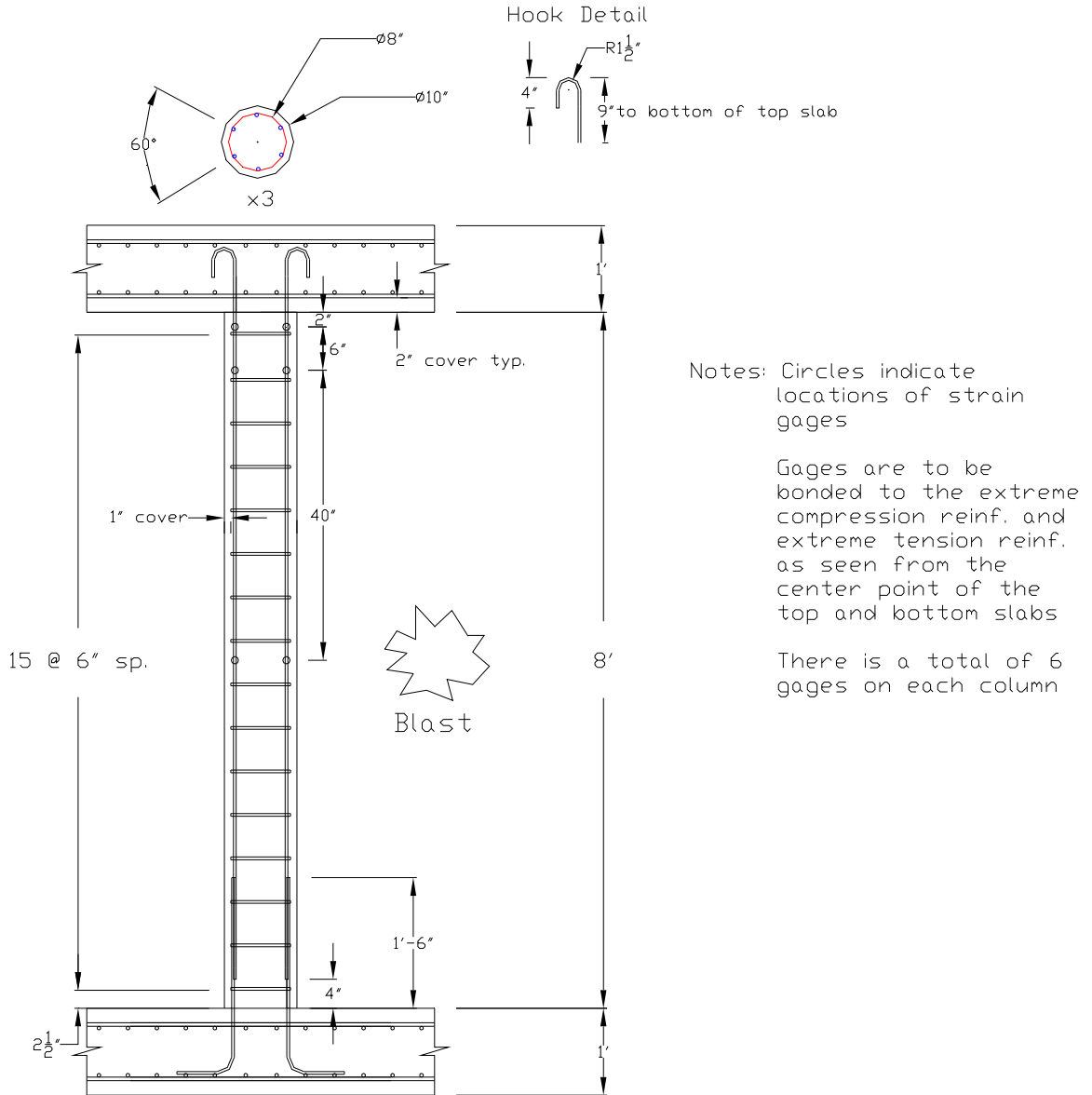


Figure A.1. Column Reinforcement Details

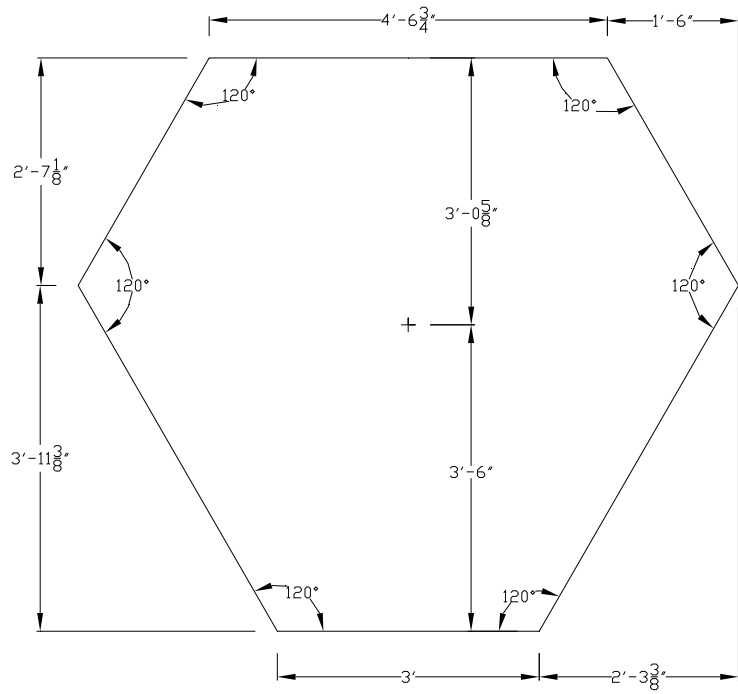


Figure A.2. Dimensions of Footing and Slab

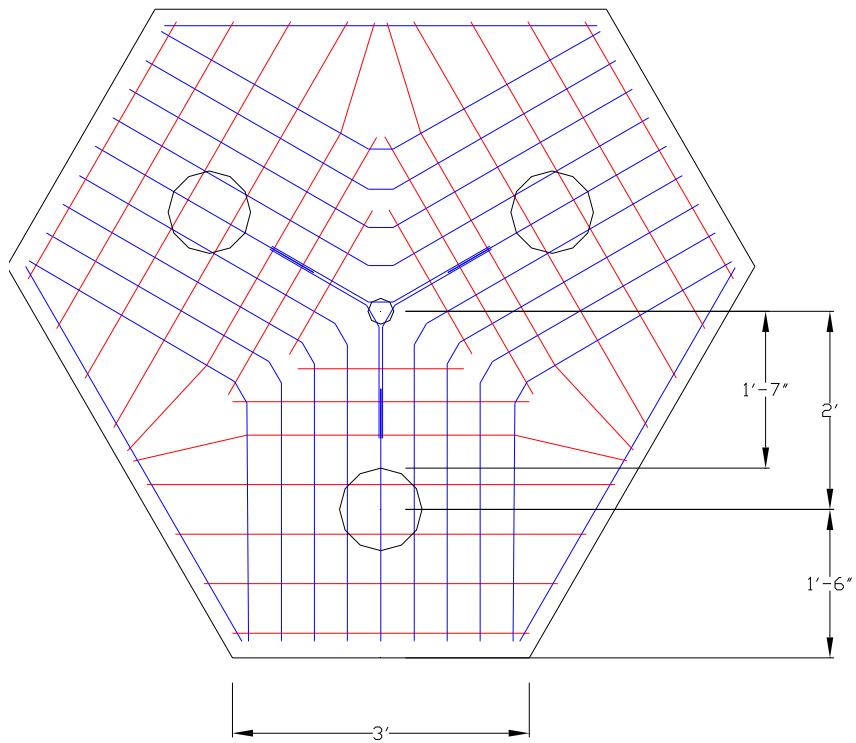


Figure A.3. Reinforcement Details for Footing and Slab

## A.2 USC\_RC Column Analysis Results

The RC column has a concrete compressive strength of 5.3 ksi, steel modulus of elasticity of 29000 ksi, steel yield strength of 66 ksi, and steel ultimate strength of 90 ksi. To take into account the strain-rate effect approximately, the dynamic increase factors specified in TM5-1300 are considered. They are 1.25, 1.23, and 1.05 for concrete compressive strength, steel yield strength, and steel ultimate strength, respectively. The Mander confinement model was used for the effect of steel ties.

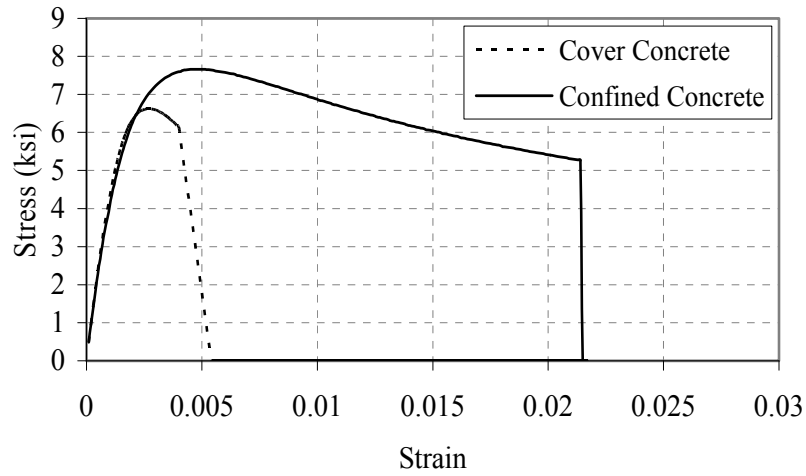


Figure A.4. Stress-Strain Relationship for Concrete

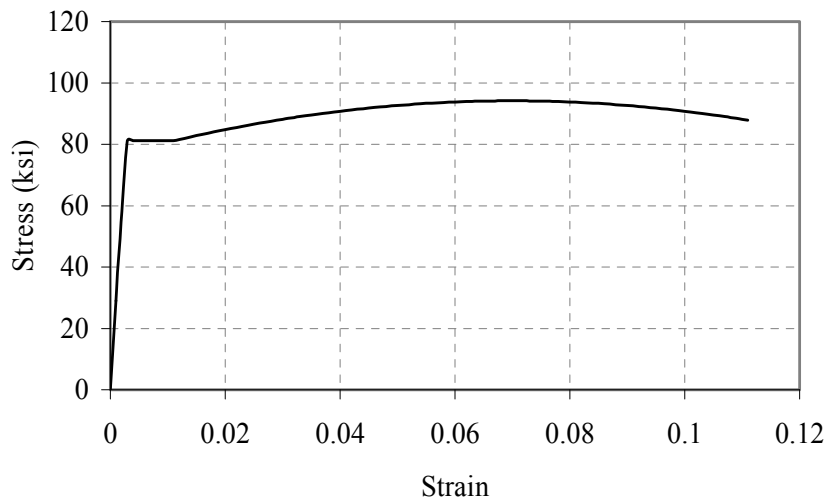


Figure A.5. Stress-Strain Relationship of Rebar

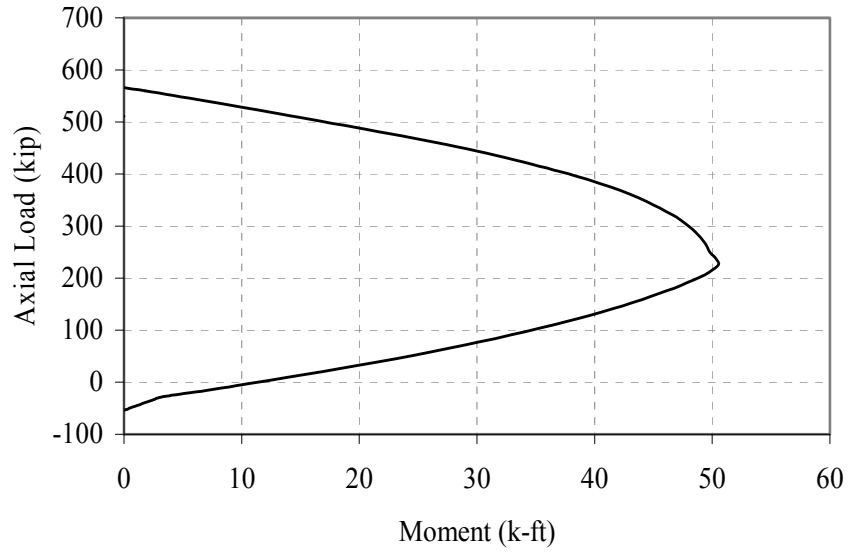


Figure A.6. Column Interaction Diagram

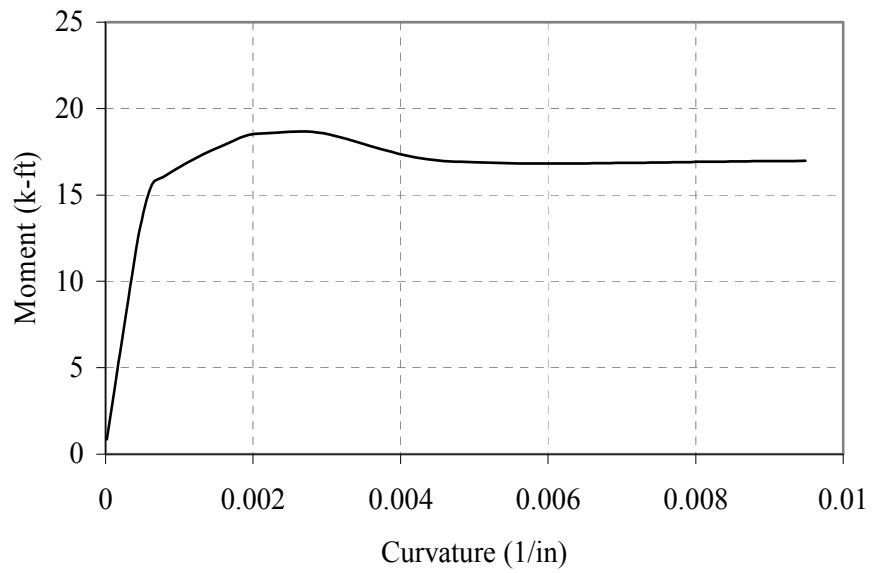


Figure A.7. Moment Curvature Diagram

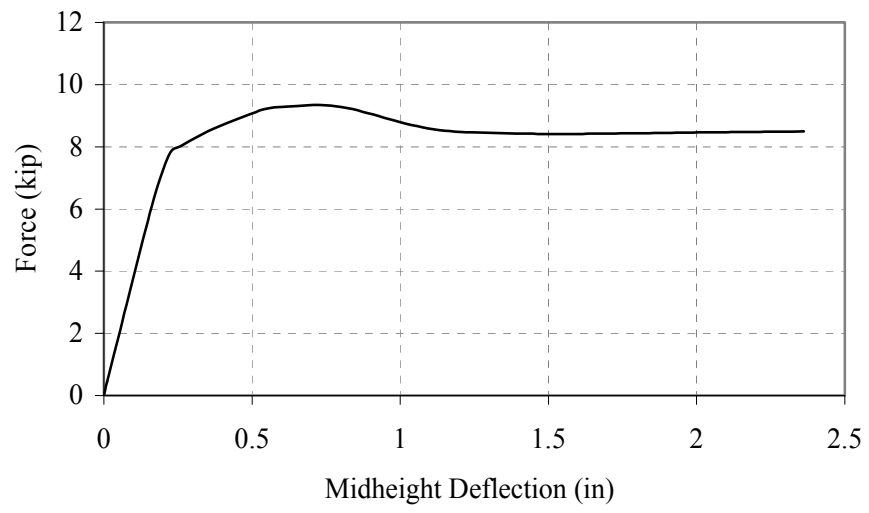


Figure A.8. Force-Deflection Diagram for a Point Load at Mid-height